



Facile synthesis of hollow zeolite microspheres through dissolution–recrystallization procedure in the presence of organosilanes

Haixiang Tao, Jiawen Ren, Xiaohui Liu, Yanqin Wang*, Guanzhong Lu*

Shanghai Key Laboratory of Functional Materials Chemistry, Research Institute of Industrial Catalysis, East China University of Science and Technology, Shanghai 200237, PR China

ARTICLE INFO

Article history:

Received 9 November 2012

Received in revised form

23 January 2013

Accepted 28 January 2013

Available online 5 February 2013

Keywords:

Zeolite

Hollow structure

Hydrothermal synthesis

Organosilane

Dissolution–recrystallization

ABSTRACT

Hollow zeolite microspheres have been hydrothermally synthesized in the presence of organosilanes via a dissolution–recrystallization procedure. In the presence of organosilanes, zeolite particles with a core/shell structure formed at the first stage of hydrothermal treatment, then the core was consumed and recrystallized into zeolite framework to form the hollow structure during the second hydrothermal process. The influence of organosilanes was discussed, and a related dissolution–recrystallization mechanism was proposed. In addition, the hollow zeolite microspheres exhibited an obvious advantage in catalytic reactions compared to conventional ZSM-5 catalysts, such as in the alkylation of toluene with benzyl chloride.

Crown Copyright © 2013 Published by Elsevier Inc. All rights reserved.

1. Introduction

Hollow microspheres with various components have drawn extensive attention for their application in controlled drug delivery, separation, catalysis, microreactors and so on [1–7]. Among these hollow microspheres, hollow silica microspheres commonly with mesoporous shells are greatly favored, due to their advantages in mass diffusion and transport resulting from their large volume and mesoporous channels on the shell. However, the shells of these hollow silica microspheres are amorphous, which may limit their applications in severe circumstance.

Zeolites are a series of crystalline aluminosilicates which are widely used in heterogeneous catalysis, especially in petroleum and oil refining because of their high acidity and shape-selectivity induced by molecular-sized microporosity [8–10]. Recently, there has been great interest in the fabrication of hollow zeolite structures with mesoporous walls. Up to now, a variety of hard templates such as polystyrene spheres [11–13], spherical CaCO_3 [14], and mesoporous silica spheres [15–20] have been utilized to prepare hollow zeolite spheres. Based on electrostatic interaction, zeolite nanocrystals or seeds were deposited on the exterior surfaces of hard templates (known as layer-by-layer assembly); therefore, the morphology and size of hollow zeolite spheres are highly dependent on the hard template and the subsequent LBL

technique, which involved complicate multistep and time-consuming processes. Recently, Shi et al. [21] reported that hollow zeolite microspheres with a close packed nanozeolite shell can be obtained by an improved polymerization-induced colloid aggregation method. Hasan et al. [22] obtained LTA zeolite crystals with multi-hollow polycrystalline core-shell structure via aggregation–recrystallization route in presence of emulsion droplets. Zhao et al. [23] reported the direct fabrication of mesoporous zeolite with a hollow spherical/ellipsoidal capsule structure by carefully controlling the hydrolysis temperature of TEOS and the hydrothermal treatment in the presence of conventional TPAOH and CTAB as soft micro- and mesopore generating templates. In addition, Zeolite spheres with hollow structures were also obtained from systems based on a surface to core crystallization mechanism. Chen et al. [24] obtained zeolite analcime with a core-shell and hollow icositetrahedron architecture in the presence of ethylamine and Raney Ni. Wang et al. [25] synthesized core/shell ZSM-5 spheres with hollow structures through in situ transformation of mesoporous silica spheres into MFI-type zeolite with the assistance of isopropylamine as a structure-directing agent. It is well known that an Al distribution gradient exists in zeolite crystals, some authors took advantage of this property to produce hollow ZSM-5, for instance, Groen et al. [26] generated hollow ZSM-5 crystals through controlled desilication of ZSM-5 crystals. Zhou et al. [27] obtained uniform hollow zeolite microspheres with hierarchical macro-/meso-/microporosity by an efficient post steam-assisted crystallization and mild alkaline etching approach. In addition, zeolites with hollow structures were also synthesized via a dissolution–recrystallization process. Wang et al. [28] reported the synthesis of hollow TS-1

* Corresponding authors. Fax: +86 21 64252923.

E-mail addresses: wangyanqin@ecust.edu.cn (Y. Wang), gzhu@ecust.edu.cn (G. Lu).

crystals with large intra-crystalline voids from a preferential dissolution of the conventional TS-1 crystal core by a post-synthesis treatment of the calcined zeolite crystals with highly alkaline TPAOH solutions, due to a lower crystallinity as compared to the external shell. ZSM-5 with very regular hollow architectures were also synthesized from a preferential dissolution of the core of the crystals, followed by a re-crystallization in the presence of templating molecules [29].

Herein, we report a facile method for the synthesis of hollow zeolite microspheres (HZS) in the presence of organosilanes via a dissolution–recrystallization procedure. Based on the desilication mechanism, excessive sodium hydroxide was added into a conventional zeolite synthesis system. At the first stage of crystallization, zeolite microspheres with a core/shell structure were formed in the presence of organosilanes, hollow zeolite microspheres with zeolite nanocrystals aggregated structures were fabricated at the second stage of hydrothermal treatment via a dissolution–recrystallization procedure. In addition, the acidic properties of the hollow zeolite microspheres were characterized by NH_3 -TPD and pyridine-adsorbed FT-IR, the probe reactions involving large and small molecules were used to compare the catalytic performance of hollow zeolite microspheres with conventional zeolite ZSM-5. As compared to the layer-by-layer technique and conventional dissolution–recrystallization process, this synthesis method is very simple and convenient, for the whole dissolution–recrystallization procedure was processed only in the mother liquid, which can avoid the complicate multistep and time-consuming processes in the layer by layer technique and the calcination of the parent zeolites before dissolution–recrystallization treatment (conventional dissolution–recrystallization process).

2. Experimental section

2.1. Synthesis of hollow zeolite microspheres

Hollow zeolite microspheres were synthesized using the commercial organosilanes (FY-4903) from the Guangzhou fluorine reason silicon science and technology limited company without further purification. In a typical synthesis, 0.082 g of NaAlO_2 , 4.06 g of tetrapropylammonium hydroxide (TPAOH, 25 wt%) and 0.16 g of NaOH were dissolved in 14.4 g of deionized water, the temperature of the solution was raised and kept at 80 °C. Then, 4.17 g of tetraethyl orthosilicate (TEOS) and 0.8 g of organosilanes were added to this solution, the resulting mixture was continuously stirred for an additional 2 h to obtain a homogeneous mixture. The mixture was then transferred to a stainless-steel, Teflon-lined autoclave and crystallized at 140 °C for 2 days, then the autoclave was quenched to room temperature and kept for several hours, followed by the second hydrothermal treatment at 120 °C for 3 days. Finally, the resulting product was recovered by filtration, washed with deionized water and dried in an oven at 100 °C over night. To remove the templates completely, the product was first calcined at 350 °C for 5 h, then calcined at 650 °C for 5 h with a rate of 1 °C min^{-1} , this hollow zeolite microspheres sample is designated as HZS. The samples obtained at various crystallization time in the presence of organosilane are designated as S-0 to S-6 (see Table 1 in detail). Sample obtained without organosilane under the same condition of HZS was denoted as S. In addition, conventional ZSM-5 was also synthesized according to Ref. [30].

2.2. Characterizations

Powder XRD patterns were recorded on a Bruker D8 FOCUS diffractometer using $\text{CuK}\alpha$ radiation (40 kV and 40 mA) with the scanning rate of 6° min^{-1} . Nitrogen adsorption and desorption

isotherms were measured at –196 °C with a Micromeritics ASAP 2020 M sorption analyzer. Before measurements, the samples were outgassed at 300 °C for 6 h. The scanning electron microscopy (SEM) was collected on a Hitachi S-4800 microscope operating at 15 kV. TEM images were obtained from JEM-2010 instrument operating at 200 kV. ^{27}Al MAS NMR spectra were recorded on a Bruker DRX-400 Spectrometer equipped with a magic angle spin probe at room temperature. The compositions of various samples were determined by inductively coupled plasma atomic emission spectrometry (ICP-AES) on a Thermo Scientific IRIS Intrepid spectrometer. Pyridine-adsorbed FT-IR spectra were carried out on a Nicolet Model 710, the samples were grounded into fine powders and pressed into very thin self supporting wafers. The discs were mounted in a quartz IR cell equipped with a CaF_2 window and a vacuum system. Prior to adsorption, the samples were pretreated in situ at 500 °C for 2 h under evacuation, then cooled to 50 °C where pyridine vapor was introduced into the cell for 0.5 h. The physically adsorbed pyridine was removed by evacuating at 50 °C for 1 h, after that, the sample was heated in vacuum for 1 h at 100 °C, and a spectrum was recorded. Temperature-programmed desorption of ammonia (NH_3 -TPD) was performed by using a homemade apparatus PX200 (Tianjin Golden Eagle Technology Limited Corporation). The sample (50 mg) was pretreated at 550 °C for 2 h and then cooled down to 50 °C under a N_2 flow. Pure NH_3 was injected until adsorption saturation was reached, followed by a flow of N_2 for 1 h at 90 °C. Then the temperature was raised from 90 °C to 550 °C with a heating rate of 10 °C min^{-1} and the amount of desorbed ammonia was detected by using thermal conductivity detector (TCD) at 110 °C.

2.3. Catalytic characterization

All the samples (ZSM-5) were transferred to H^+ type ZSM-5 by ion exchange with NH_4NO_3 (1 mol L^{-1}) at 80 °C for 3 h, which repeated three times, finally all the samples were calcined at 550 °C for 3 h.

2.4. Acetalization of cyclohexanone

The acetalization of cyclohexanone was carried out batch-wise in a round-bottomed flask equipped with a flux condenser and a magnetic stirrer. In a typical reaction, 0.05 g of catalyst (H^+ form) was dispersed in a solution containing 10 mL of methanol and 0.098 g of cyclohexanone. The solution was stirred at 50 °C for 4 h. The reaction mixtures were analyzed by a Perkin-Elmer Clarus 500 gas chromatography with a SE-54 column. The product mixture was further confirmed by GC–MS.

2.5. Alkylation of toluene with benzyl chloride

The catalytic reactions were carried out under N_2 in a three-necked flask equipped with a reflux condenser. In a typical run, 1.38 g of toluene, 1.9 g of benzyl chloride and 0.05 g of catalyst were mixed with stirring, then the reaction temperature was raised to and kept at 80 °C for 3 h. The reaction mixtures were separated by centrifugation and analyzed by a Perkin-Elmer Clarus 500 gas chromatography with a SE-54 column. The product was further confirmed by GC–MS.

3. Results and discussion

Hollow zeolite microspheres (HZS) were synthesized by adding organosilane to a conventional hydrothermal system via a dissolution–recrystallization procedure. X-ray powder diffraction

Table 1
Textural parameters of various samples at different hydrothermal conditions.

Samples	Hydrothermal conditions	Si/Al ratio ^a	S_{BET} [$\text{m}^2 \text{g}^{-1}$]	S_{micro} [$\text{m}^2 \text{g}^{-1}$] ^b	V_{total} [$\text{cm}^3 \text{g}^{-1}$]	V_{meso} [$\text{cm}^3 \text{g}^{-1}$]	V_{micro} [$\text{cm}^3 \text{g}^{-1}$] ^b
HZS	140-2 and 120-3 ^c	30	353.4	253.5	0.25	0.13	0.12
S	140-2 and 120-3	19	354.9	270.1	0.22	0.09	0.13
S-0	Without aging	32	14.1	4.6	0.02	0.02	–
S-1	140-0.5	29	127.4	90.7	0.07	0.03	0.04
S-2	140-1	29	256.4	173.0	0.14	0.06	0.08
S-3	140-2	30	271.0	174.8	0.20	0.12	0.08
S-4	140-2 & 120-1	29	341.2	244.6	0.20	0.09	0.11
S-5	140-5	31	347.5	267.3	0.19	0.07	0.12
S-6	140-7	30	358.8	254.6	0.26	0.14	0.12
S-7	140-2	28	329.7	275.1	0.16	0.03	0.13
con-ZSM-5	140-5	33	345.1	303.6	0.16	0.02	0.14

Note:

^a Measured by ICP-AES.

^b Determined by *t*-plot method.

^c 140-2 and 120-3, which means that the sample was first hydrothermal crystallized at 140 °C for 2 days, and then hydrothermal treated at 120 °C for 3 days.

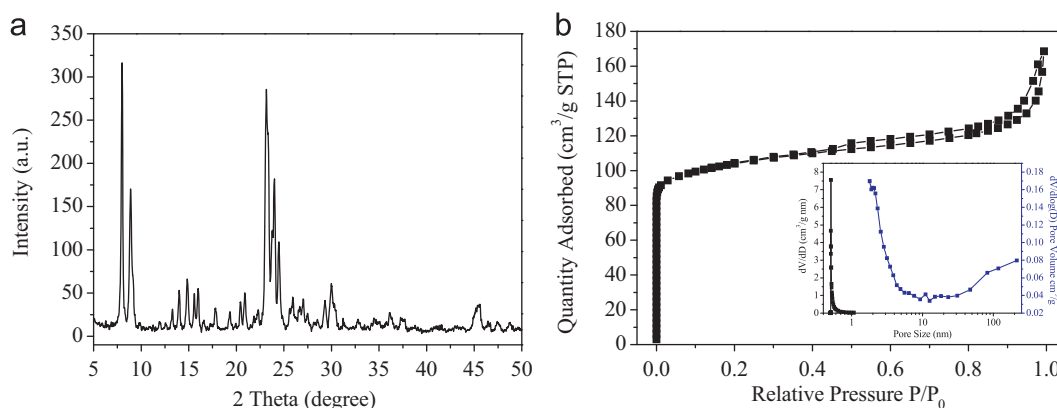


Fig. 1. Wide-angle XRD pattern (a) and N_2 adsorption–desorption isotherm (b) of HZS.

pattern of HZS clearly shows the characteristic peaks of MFI-type zeolite structure (as shown in Fig. 1a), indicating that the sample was highly crystallized. The nitrogen adsorption–desorption isotherms (Fig. 1b) of HZS exhibit a steep increase at relative pressure $P/P_0 < 0.02$ and a hysteresis loop at a relative pressure P/P_0 of 0.45–0.99, which indicates the co-existence of intrinsic micropores centered around 0.53 nm (shown in Fig. 1b inset) and mesopores. The BET surface area, micropore and mesopore volume are $353.4 \text{ m}^2 \text{ g}^{-1}$, $0.12 \text{ cm}^3 \text{ g}^{-1}$ and $0.13 \text{ cm}^3 \text{ g}^{-1}$, respectively. SEM images (Fig. 2a and b) exhibit that sample HZS (0.6–1 μm) has spherical morphology, but with rough surface. TEM images (Fig. 2c and d) demonstrate their hollow structure with a shell thickness of ca. 100 nm, the external surface of the particles is rough, which is in good agreement with SEM observation. The high-resolution TEM image of hollow zeolite spheres is taken from the edge of the shell, the lattice fringes are clearly distinguished, revealing the shell of the hollow zeolite spheres is not a single crystal but polycrystalline framework, which is consistent with the result of selected area electron pattern (Fig. 2e inset). These results confirm that the shell of HZS is composed of aggregated zeolite nanocrystals.

In order to investigate the role played by organosilane, sample S synthesized under the same condition of HZS but without organosilane was also analyzed. X-ray diffraction pattern of sample S is shown in Fig. 3a, it exhibits the characteristic diffraction peaks of MFI-type zeolite structure. The N_2 adsorption–desorption curves of sample S exhibit two steep increases at relative pressure $P/P_0 < 0.02$ and P/P_0 of 0.5–0.99, these adsorptions were interpreted as micropore filling and

capillary condensation in mesopores, respectively, indicating the co-existence of intrinsic micropores centered around 0.53 nm (shown in Fig. 3b inset) and mesopores. The BET surface area, micropore and mesopore volume are $354.9 \text{ m}^2 \text{ g}^{-1}$, $0.13 \text{ cm}^3 \text{ g}^{-1}$ and $0.09 \text{ cm}^3 \text{ g}^{-1}$, respectively. SEM and TEM images of sample S are shown in Fig. 4. Obviously, regular micrometer-sized zeolite with smooth surface was obtained, the overview of TEM images shows that well-shaped zeolites with uniform size and many brighter areas corresponding to the mesopores created by desilication under basic conditions are observed in the TEM images (shown in Fig. 4c), which can further be confirmed by the significant decrease of Si/Al ratio of sample S, as compared to sample S-7. The high-resolution TEM image of sample S is taken from the edge of well-shaped zeolite crystal, the lattice fringes are clearly distinguished, revealing the each zeolite crystal of sample S is a single crystal, which is further confirmed by selected area electron pattern (Fig. 4d inset).

Obviously, the morphology and structure of sample S are different from those of HZS, indicating that the organosilane played a dominant role on the formation of the globular morphology and hollow structure of HZS. Other samples with different amount of organosilanes were also synthesized under the same condition of HZS, these samples were designated as HZS (X), X indicates the amount of organosilanes, for example, HZS (0.2) means that 0.2 g of organosilanes were added in the synthesis system. The characterizations (XRD, SEM, TEM and Nitrogen sorption analysis are shown in supporting information, see Figs. S1–S3 in detail). The TG curves (Fig. S4) show that the weight loss of uncalcined samples [HZS (0.2), HZS (0.4), and HZS (0.8)] with different

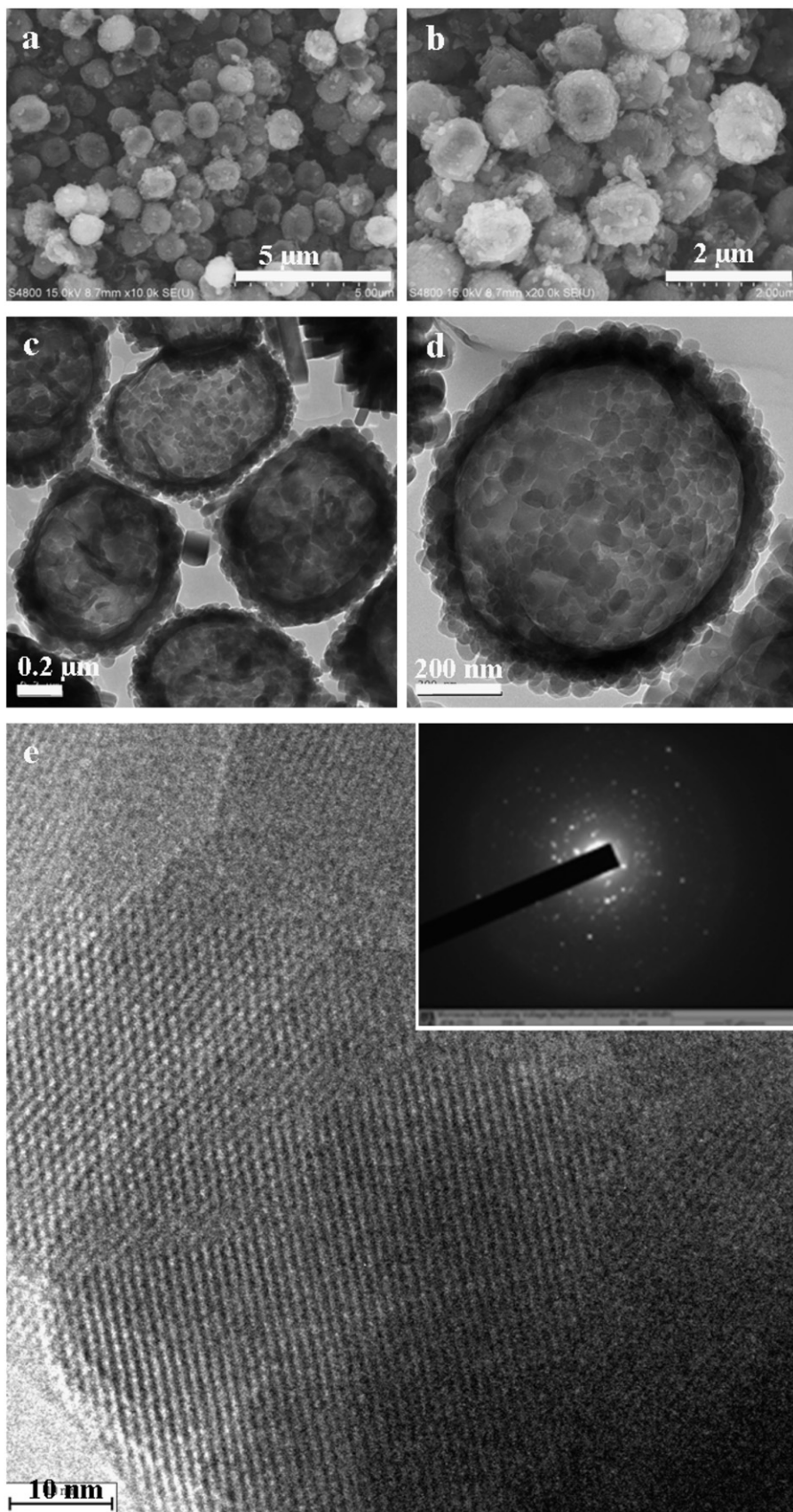


Fig. 2. SEM (a), (b) and TEM (c)–(e) images of HZS.

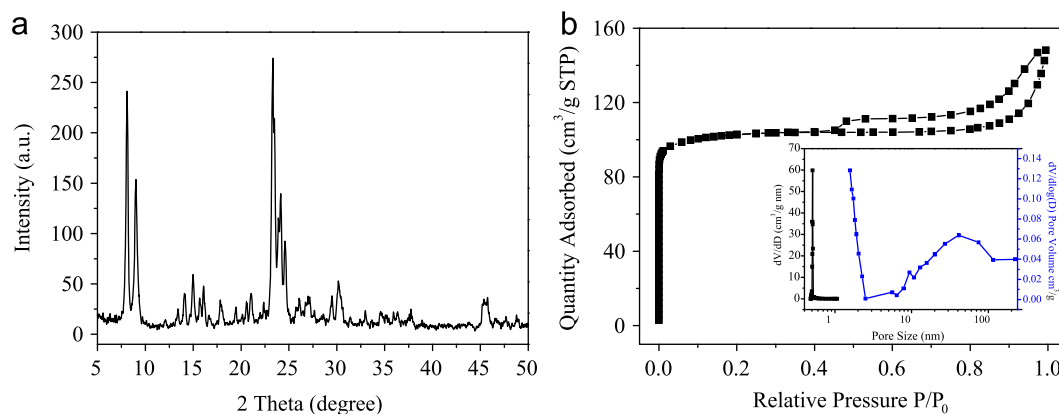


Fig. 3. Wide-angle XRD pattern (a) and N_2 adsorption-desorption isotherm (b) of sample S synthesized without organosilane.

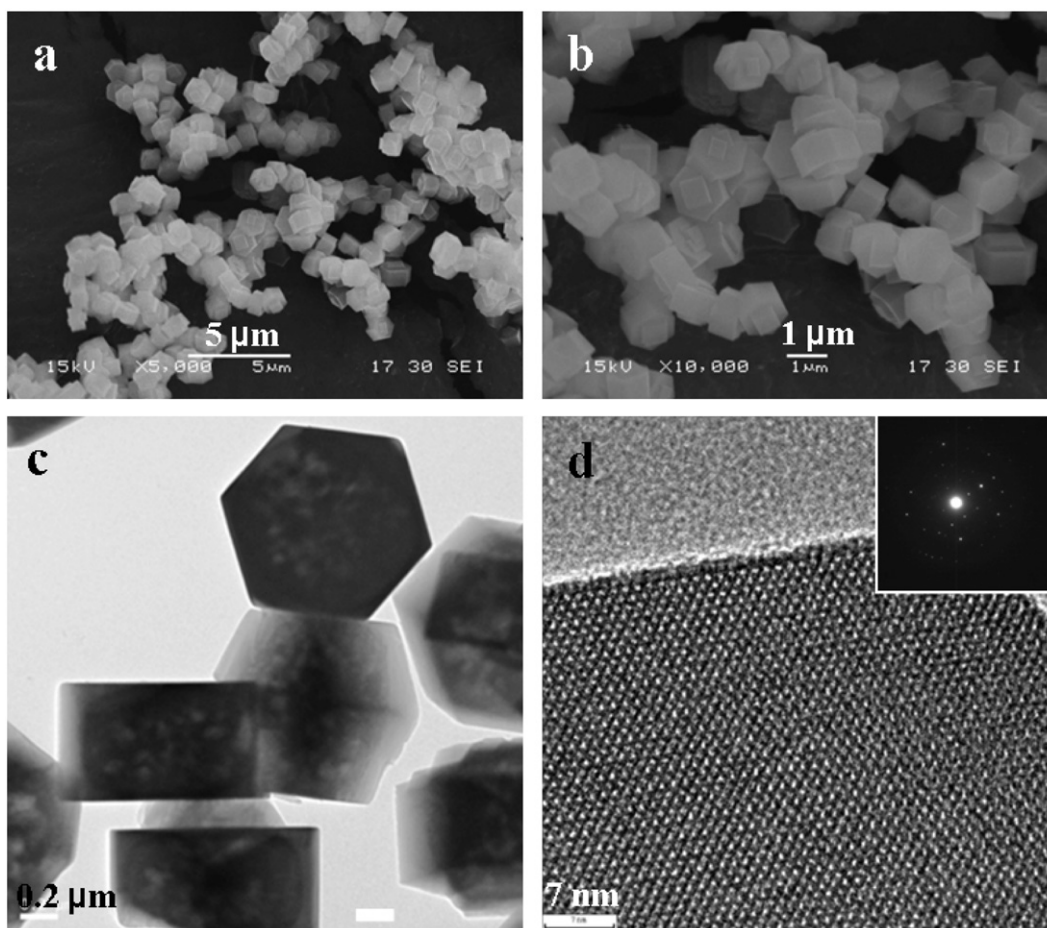


Fig. 4. SEM (a), (b) and TEM (c), (d) images of sample S synthesized without organosilane.

amount of organosilanes was more than that of sample S, suggesting that the former three samples all contained organosilanes besides TPA^+ cations, the DTG curves indicate that the one weight loss peak centered at 460°C , which originated from the decomposition of TPA^+ cations, the other one centered at 403°C is attributed to the decomposition of organosilanes, the weight loss related to the organosilanes took place at lower temperature than that of TPA^+ , suggesting that the former was located mainly on the external surface. To further investigate the formation of the hollow structure, several samples were recovered during the synthesis procedure and the physical parameters are summarized in Table 1. Fig. 5 shows the wide-angle XRD patterns of the samples at different crystalline time

at 140°C in the presence of organosilane. It is found that there is no pronounced peak in the XRD pattern of sample S-0, only a broad one at around 23° , which suggests an amorphous framework structure. For sample S-1 which was crystallized at 140°C for 12 h, the characteristic peaks of MFI-type zeolite begin to appear, which means the crystalline phase begins to form at this stage, the reflections from the amorphous framework can still be detected after 1 day (Fig. 5 inset, sample S-2), and well-defined wide-angle XRD peaks are observed after 2 days at 140°C .

Figs. 6 and 7 show representative scanning and transmission electron micrographs of the samples crystallized at 140°C for various time. SEM and TEM images reveal that the amorphous

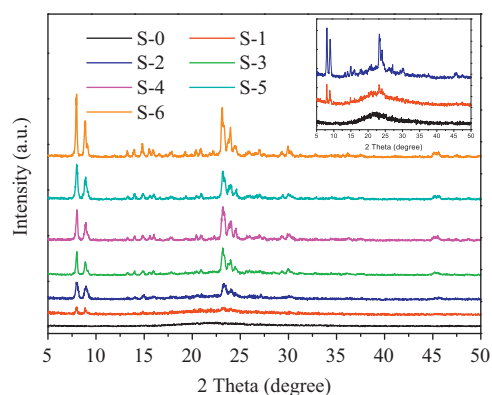


Fig. 5. Wide-angle XRD patterns of the samples obtained at various crystallization times.

aluminosilicates (S-0) do not have any regular shape and size before crystallization, and almost no mesoporous structure can be observed at this stage (as shown in Figs. 6 and 7a), which is in good agreement with the results of N_2 sorption measurement ($S_{BET}=14\text{ m}^2\text{ g}^{-1}$, $V_{total}=0.02\text{ cm}^3\text{ g}^{-1}$). This means that the organosilane does not act as a mesopore structure-directing agent. Interestingly, the morphology drastically changes during the crystallization at the first 12 h, the regular spherical particles ($1\text{ }\mu\text{m}$) with relatively smooth surface are formed at this stage, and the TEM images of S-1 reveal that most of these particles are connected with each other, the amount of isolated particles is small (as shown in Fig. 7b), which is consistent with the SEM observation (Fig. 6b). With the prolonging of the crystallization time (1 day), the globular morphology of S-2 remains unchanged, but the surface of the particles become rougher. Interestingly, TEM images (Fig. 7C inset) of S-2 show that some particles

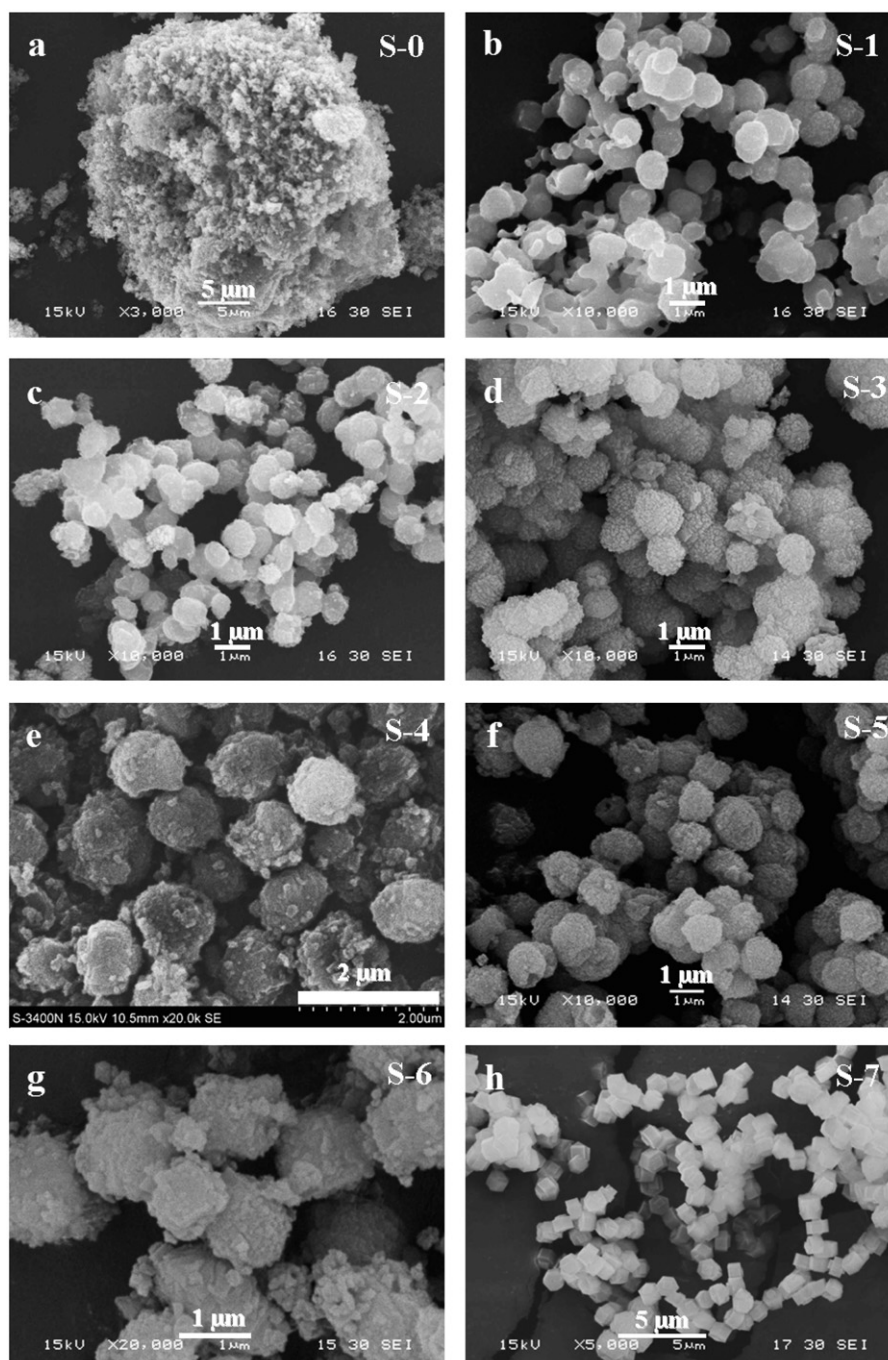


Fig. 6. SEM images of the products obtained at various crystallization times.

possess a core/shell structure, most of S-2 still have a spherical morphology, but with a rough external surface. After 2 days of crystallization (sample S-3), almost all of the particles possess a core/shell structure, the morphology and structure of these particles (S-3) is similar to the report for hierarchical zeolites grown by another organosilane template by Koekkoek et al. [31]. The high-resolution TEM image of S-3 taken from the edge of the shell (Fig. 6e), the lattice fringes are clearly distinguished, revealing high crystallinity of these nano-particles, which can be further confirmed by selected area electron pattern (Fig. 7d inset), the BET surface area and micropore volume of S-3 are increased to $271 \text{ m}^2 \text{ g}^{-1}$ and $0.08 \text{ cm}^3 \text{ g}^{-1}$, respectively. Micropore volumes have often been used as an indicator for the crystallinity of MFI zeolites [32,33]. From the viewpoint of micropore volume, S-3 is not well crystallized, it is reasonable to speculate that the core of S-3 is not well crystallized, in another word, S-3 still contains a non-negligible amount of the amorphous phase. After quenching to room temperature, sample S-4 was further crystallized at 120°C for 1 day (the second step), sample S-4 remains the spherical morphology, but the core of the spheres was partially dissolved (Fig. 7f), leading to a hollow structure. In addition, the size of nano-particles of S-4 is a little larger than that of S-3, which means that the dissolved species were recrystallized and re-assembly on the zeolite framework to form a little denser external shell, the micropore volume of S-4 increased up to $0.11 \text{ cm}^3 \text{ g}^{-1}$. With the prolongation of hydrothermal treatment to 3 days at 120°C , zeolite microspheres with completely hollow structure were fabricated (Fig. 2). On the other hand, when the crystallization time is increased up to 5 days (at 140°C) without quenching to room temperature, zeolite spheres without any dissolved core were observed in the TEM image (Fig. 7g). With

the prolongation of crystallization time up to 7 days (at 140°C), well crystallized zeolite spheres were observed in the TEM image, and the N_2 sorption measurement reveals that the micropore volume of sample S-6 is $0.12 \text{ cm}^3 \text{ g}^{-1}$, indicating high crystallinity of sample S-6. The reference sample S-7 was obtained without organosilane at 140°C for 2 days, SEM and TEM images (Fig. 6h and Fig. 7i) show that regular micrometer-sized zeolite with a coffin-like morphology was obtained, and no mesopores were observed in the TEM image. The Si/Al ratio of sample S-7 is 28, which is similar to all the samples obtained in the presence of organosilane, but much higher than the Si/Al ratio (19) of sample S. The N_2 sorption isotherms of all samples are shown in

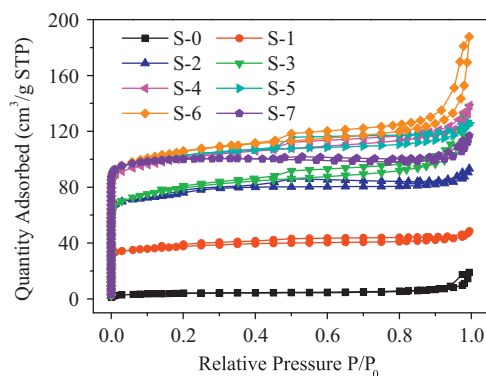


Fig. 8. N_2 adsorption–desorption isotherms of products obtained at various crystallization times.

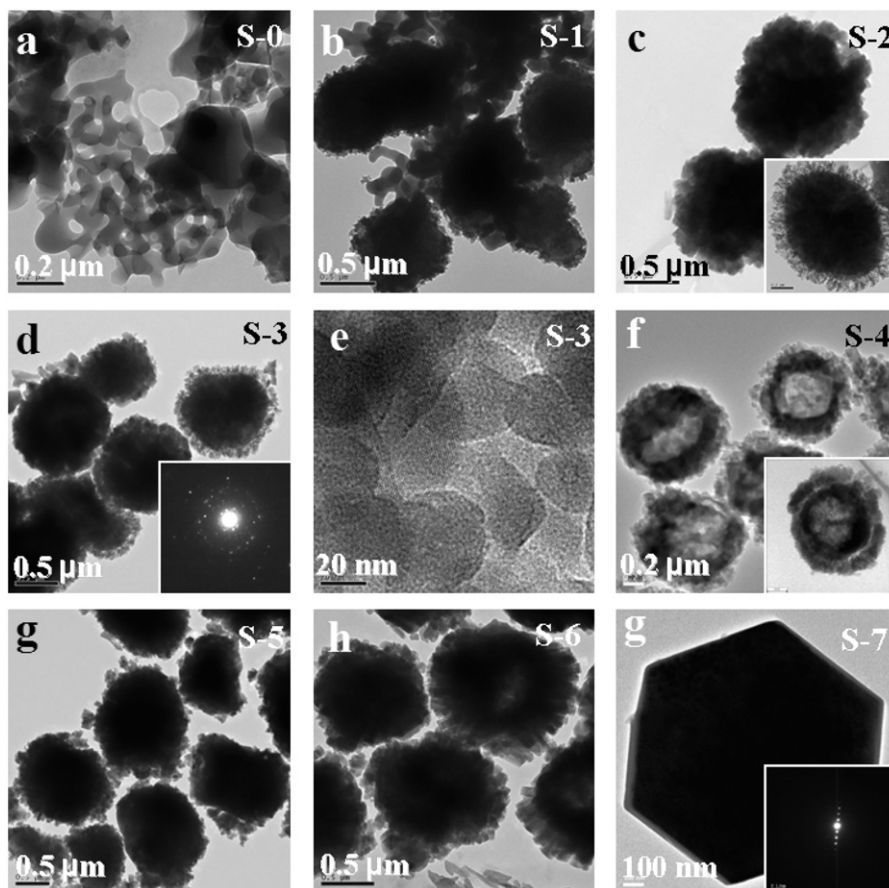


Fig. 7. TEM images for products obtained at various crystallization times.

Fig. 8. and the textural parameters of all samples are summarized in Table 1.

^{27}Al MAS NMR spectra of the samples recovered during the synthesis procedure are used for comparison and shown in Fig. 9. Before crystallization, a single broad peak at around 0–65 ppm was observed, indicating tetrahedral Al and extra-framework Al both exist in the amorphous phase of S-0. During the crystallization process, peak at 55 ppm becomes sharper and the signal around 0–10 ppm decreases in intensity and even disappears after 2 days of crystallization, which means that the extra-framework Al were incorporated into the zeolite framework during hydrothermal treatment procedure.

The formation of the hierarchical hollow zeolite spheres is schematically illustrated in Scheme 1 and can be described as follows: (1) Step I: microspheres with size of 0.6–1 μm are formed in the presence of organosilanes during the crystallization of 0.5 day, with the crystallization time prolonged to 2 days, aluminosilicate species in solution are crystallized to form zeolite nanocrystals, and these nanocrystals are self-assembled and deposited on the external surface of microspheres to form the core/shell structure. It is reported that organosilanes can be anchored on the surface of zeolite nanocrystals through the covalent Si–O–Si linkages, which can slow down the growth of the zeolite nanocrystals (as shown in Scheme 1 right top). (2) Step II: During this process, the sample was quenched to room temperature and hydrothermal treated at a lower temperature. It is well known that temperature has a major influence on the crystallization of ZSM-5 zeolite, and silica species can be dissolved at relatively low temperature [29]. Therefore, the crystallization of MFI-type zeolite is almost stopped at room temperature, during the process of increasing the temperature, the crystallization rate (R_c) is much smaller than the dissolution rate (R_d), as a result, the amorphous aluminosilicate cores can be

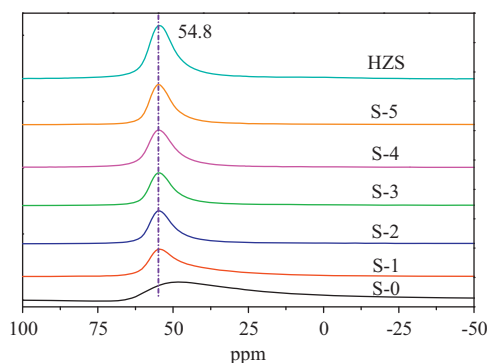
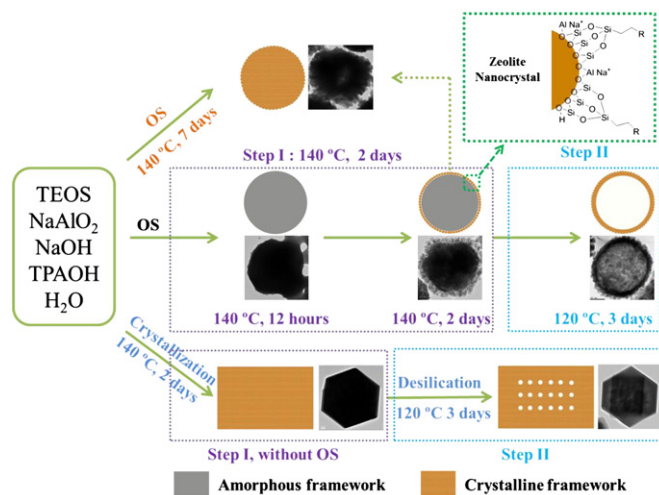


Fig. 9. ^{27}Al MAS NMR spectra of products obtained at various crystallization times.

dissolved, leaving a large cavity, and these dissolved species can be further recrystallized into zeolite framework and deposited on the nanocrystals to form the denser zeolite shell. In order to prove the amorphous framework of the core is the main reason to the formation of the hollow structures, STEM and elemental analysis were used to investigate the aluminum and silica distribution in the sample, S-3 (Fig. 10), both silica and aluminum distributed evenly in the whole particle, confirming that the formation of the hollow structure is attributed to the amorphous framework in the core rather than the Al distribution gradient exists in zeolite crystals. In addition, during the prolonged hydrothermal period, the size of small amount of zeolite nanocrystals increased due to a ripening process by consuming the dissolved aluminosilicate species, especially for the external surface of the shell, such phenomenon is similar to the report for hierarchical zeolites grown by another organosilane template [34]. At last, the hollow structure can be fabricated via a dissolution–recrystallization procedure. On the other hand, when the sample was continuously crystallized at 140 $^{\circ}\text{C}$ for 7 days, the crystallization rate (R_c) is similar to the dissolution rate (R_d), well-crystallized zeolite spheres were formed. While zeolite single crystal was obtained in the absence of organosilanes, during the second hydrothermal stage, the silicon can be selectively dissolved in basic media.

Fig. 11 shows the curves of the temperature-programmed desorption of ammonia for various ZSM-5 samples (Both samples are H^+ form). All the ZSM-5 catalyst show two desorption peaks of NH_3 in the range below 550 $^{\circ}\text{C}$, these desorption peaks were corresponding to two different type of acid sites of varying strengths. The low



Scheme 1. Schematic illustration of the formation of the structural changes of hollow zeolite spheres during crystallization procedure.

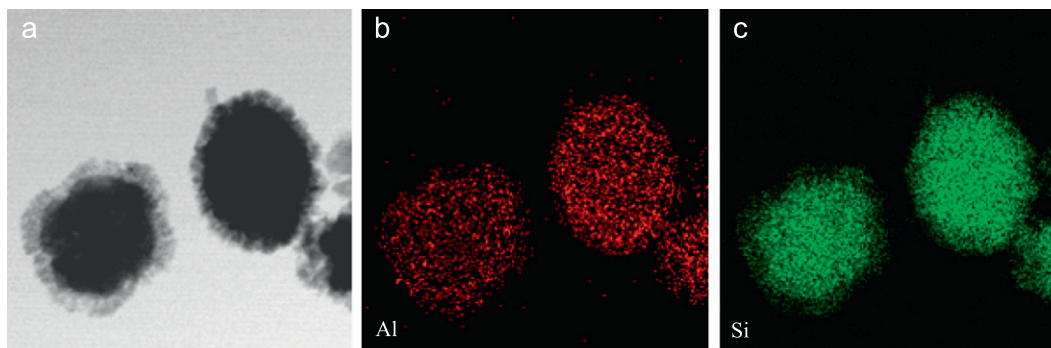


Fig. 10. STEM images (a) and EDX element mapping of aluminum (b) and silica (c) for sample S-3.

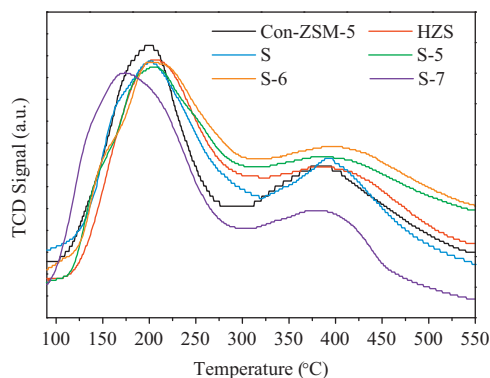


Fig. 11. NH_3 -TPD curves of various ZSM-5 samples.

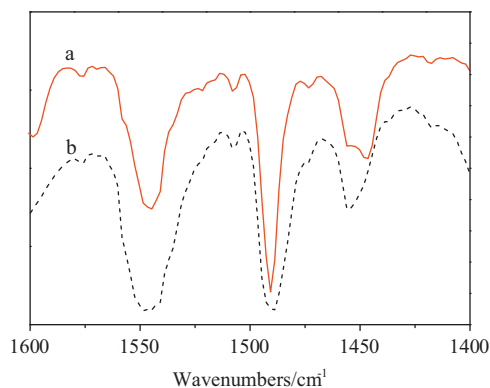
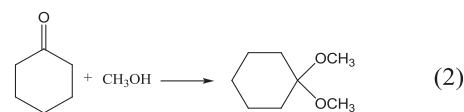
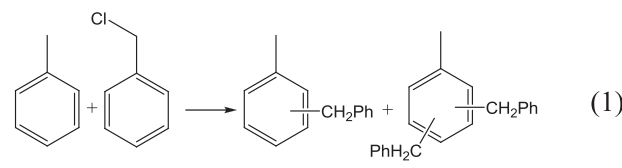


Fig. 12. FT-IR spectra of HZS (a) and Con-ZSM-5 (b) obtained after adsorption of pyridine at 100 °C.

temperature desorption peak indicates weak adsorption acidic sites, and the peak at high temperature is attributed to the interaction of NH_3 with strong acidic sites. Fig. 12 shows the pyridine adsorbed FT-IR spectra in 1400–1600 cm^{-1} for HZS and conventional ZSM-5. There are three bands in the region. The one at about 1450 cm^{-1} arising from the C–C stretch of a coordinatively bonded pyridine complex indicates the presence of Lewis acid sites. The 1540 cm^{-1} one is attributed to the C–C stretching vibration of the pyridinium ion and has been used for the identification of the Brønsted acid sites. The other at about 1490 cm^{-1} is attributed to the pyridine species interacting with both the two kinds of acid sites.

Alkylation of toluene with benzyl chloride (reaction 1) and acetalization of cyclohexanone with methanol (reaction 2) were performed to verify the catalytic activity of various ZSM-5 catalysts. The reaction results obtained are summarized in Table 2. In the reaction (1) involving large molecules, ZSM-5 catalysts with secondary mesopore structures (HZS, S, S-5, S-6) were found to be highly active compared to Con-ZSM-5 and S-7, for example, the highest toluene conversion (49.8%) is achieved over HZS catalysts, the reference sample con-ZSM-5 (24.8%) displays the lowest conversion, the similar toluene conversion (29.3%) was obtained over S-7 sample. On the other hand, for the reaction (2) involving small molecules, similar cyclohexanone conversions (84–88.5%) were obtained over all the ZSM-5 catalysts. However, the details of the acidity of those active sites and the distribution of them in the mesopores and micropores are not clear for now, it may be reasonable to presume that one of key factors responsible for the improved catalytic performances in the catalytic reactions involving large molecules is the improved mass diffusion, resulting from the presence of secondary mesopore structure and large external surface areas.

Table 2
Catalytic performance of various ZSM-5 catalysts.



Samples	Reaction 1	Reaction 2
	Toluene conversion (%)	Cyclohexanone conversion (%)
con-ZSM-5	24.8	84.1
HZS	49.8	87.8
S	47.9	88.5
S-5	39.6	85.7
S-6	43.0	88.0
S-7	29.3	84.0

4. Conclusion

In summary, hierarchical hollow zeolites microspheres with zeolite nanocrystals aggregated structures have been obtained by adding organosilanes to a conventional zeolite synthesis route via a dissolution–recrystallization procedure. As compared to the previous synthesis methods including the layer-by-layer technique and conventional dissolution–recrystallization procedure, this synthesis method is simple and convenient, for the whole dissolution–recrystallization procedure was processed only in the mother liquid, which can avoid the complicate multistep and time-consuming processes in the layer by layer technique and the calcination of the parent zeolites before dissolution–recrystallization treatment. This hollow zeolite microspheres exhibit high surface area, large mesopore volume and strong acidity, and display a clear advantage on catalysis reactions compared to conventional ZSM-5 catalysts, especially for the reactions involving large molecules. Further more, this simple method could be easily extended to prepare other MFI type zeolites with hollow structures, such as hollow Silicalite-1 and Hollow TS-1 (Figs. S5 and S6).

Acknowledgments

This project was supported financially by the 973 Program of China (2010CB732300), the National Natural Science Foundation of China (No. 20973058, 21273071), the Science and Technology Commission of Shanghai Municipality (10dz2220500) and the Fundamental Research Funds for the Central Universities, China.

Appendix A. Supporting information

Supplementary data associated with this article can be found in the online version at <http://dx.doi.org/10.1016/j.jssc.2013.01.045>.

References

- [1] Y.J. Wang, A.S. Angelatos, F. Caruso, Chem. Mater. 20 (2008) 848–858.
- [2] K.P. Gierszal, M. Jaroniec, J. Am. Chem. Soc. 128 (2006) 10026–10027.
- [3] Y. Zhao, L. Jiang, Adv. Mater. 21 (2009) 3621–3638.

- [4] R. Liu, S.M. Mahurin, C. Li, R.R. Unocic, J.C. Idrobo, H.J. Gao, S.J. Pennycook, S. Dai, *Angew. Chem. Int. Ed.* 50 (2011) 6799–6802.
- [5] Y.F. Zhu, J.L. Shi, W.H. Shen, X.P. Dong, J.W. Feng, M.L. Ruan, Y.S. Li, *Angew. Chem. Int. Ed.* 44 (2005) 5083–5087.
- [6] X. Gu, C.L. Li, X.H. Liu, J.W. Ren, Y.Q. Wang, Y.L. Guo, Y. Guo, G.Z. Lu, *J. Phys. Chem. C* 113 (2009) 6472–6479.
- [7] J. Liu, S.B. Hartono, Y.G. Jin, Z. Li, G.Q. Lu, S.Z. Qiao, *J. Mater. Chem.* 20 (2010) 4595–4601.
- [8] M.E. Davis, *Nature* 417 (2002) 813–821.
- [9] C.S. Cundy, P.A. Cox, *Chem. Rev.* 103 (2003) 663–701.
- [10] A. Corma, *Chem. Rev.* 97 (1997) 2373–2419.
- [11] X.D. Wang, W.L. Yang, Y. Tang, Y.J. Wang, S.K. Fu, Z. Gao, *Chem. Commun.* (2000) 2161–2162.
- [12] V. Valtchev, S. Mintova, *Microporous Mesoporous Mater.* 43 (2001) 41–49.
- [13] V. Valtchev, *Chem. Mater.* 14 (2002) 4371–4377.
- [14] D.J. Wang, G.B. Zhu, Y.H. Zhang, W.L. Yang, B.Y. Wu, Y. Tang, Z.K. Xie, *New J. Chem.* 29 (2005) 272–274.
- [15] A.G. Dong, Y.J. Wang, Y. Tang, N. Ren, Y.H. Zhang, Z. Gao, *Chem. Mater.* 14 (2002) 3217–3219.
- [16] A.G. Dong, N. Ren, W.L. Yang, Y.J. Wang, Y.H. Zhang, D.J. Wang, J.H. Hu, Z. Gao, Y. Tang, *Adv. Funct. Mater.* 13 (2003) 943–948.
- [17] A.G. Dong, Y.J. Wang, D.J. Wang, W.L. Yang, Y.H. Zhang, N. Ren, Z. Gao, Y. Tang, *Microporous Mesoporous Mater.* 64 (2003) 69–81.
- [18] N. Ren, B. Wang, Y.H. Yang, Y.H. Zhang, W.L. Yang, Y.H. Yue, Z. Gao, Y. Tang, *Chem. Mater.* 17 (2005) 2582–2587.
- [19] C.R. Xiong, D. Coutinho, K.J. Balkus, *Microporous Mesoporous Mater.* 86 (2005) 14–22.
- [20] J. Shi, N. Ren, Y.H. Zhang, Y. Tang, *Microporous Mesoporous Mater.* 132 (2010) 181–187.
- [21] Y. Shi, X. Li, J.K. Hu, J.H. Lu, Y.C. Ma, Y.H. Zhang, Y. Tang, *J. Mater. Chem.* 21 (2011) 16223–16230.
- [22] F. Hasan, R. Singh, P.A. Webley, *Microporous Mesoporous Mater.* 160 (2012) 75–84.
- [23] J.J. Zhao, Z.L. Hua, Z.C. Liu, Y.S. Li, L.M. Guo, W.B. Bu, X.Z. Cui, M.L. Ruan, H.R. Chen, J.L. Shi, *Chem. Commun.* (2009) 7578–7580.
- [24] X.Y. Chen, M.H. Qiao, S.H. Xie, K.N. Fan, W.Z. Zhou, H.Y. He, J. Am. Chem. Soc. 129 (2007) 13305–13312.
- [25] Z.D. Wang, Y.M. Liu, J.G. Jiang, M.Y. He, P. Wu, *J. Mater. Chem.* 20 (2010) 10193–10199.
- [26] J.C. Groen, T. Bach, U. Ziese, A.M.P. Donk, K.P. Jong, J.A. Moulijn, J. Pérez-Ramírez, *J. Am. Chem. Soc.* 127 (2005) 10792–10793.
- [27] J. Zhou, Z.L. Hua, W. Wu, Z.C. Liu, Y. Zhu, Y. Chen, J.L. Shi, *Dalton Trans.* 40 (2011) 12667–12669.
- [28] Y.R. Wang, M. Lin, A. Tuel, *Microporous Mesoporous Mater.* 102 (2007) 80–85.
- [29] Y.R. Wang, A. Tuel, *Microporous Mesoporous Mater.* 113 (2008) 286–295.
- [30] F.S. Xiao, L.F. Wang, C.Y. Yin, K.F. Lin, Y. Di, J.S. Li, R.R. Xu, D.S. Su, R. Schlögl, T. Yokoi, T. Tatsumi, *Angew. Chem. Int. Ed.* 45 (2006) 3090–3093.
- [31] A.J.J. Koekkoek, C.H.L. Tempelman, V. Degirmenci, M.L. Guo, Z.C. Feng, C. Li, E.J.M. Hensen, *Catal. Today* 168 (2011) 96–111.
- [32] B.T. Holland, L. Abrams, A. Stein, *J. Am. Chem. Soc.* 121 (1999) 4308–4309.
- [33] W.C. Yoo, X.Y. Zhang, M. Tsapatsis, A. Stein, *Microporous Mesoporous Mater.* 149 (2012) 147–157.
- [34] M. Choi, H.S. Cho, R. Srivastava, C. Venkatesan, D.H. Choi, R. Ryoo, *Nat. Mater.* 5 (2006) 718–723.